Article

Not peer-reviewed version

Research on B_4C/PEEK Composite Material Radiation Shielding

Hongxia Li *, Hongping Guo , Hui Tu , Xiao Chen , Xianghua Zeng *

Posted Date: 13 September 2024

doi: 10.20944/preprints202409.1077.v1

Keywords: radiation shielding; simulation; hardening component; B4C/PEEK; composite material

Article

Research on B_4C/PEEK Composite Material Radiation Shielding

Hongxia Li [1,2,*], Hongping Guo [1], Hui Tu [1,2], Xiao Chen [1,2] and Xianghua Zeng [1,2,*]

[1] College of Electrical, Energy and Power Engineering, Yangzhou University, Jiangsu Yangzhou, 225009, China
[2] Innovation Center for Radiation Application, Beijing, 102413, China
* Correspondence: lihongxia@yzu.edu.cn (H.L.); xhzeng@yzu.edu.cn (X.Z.)

Abstract: There are various types of charged particles in the space environment, which can cause different types of radiation damage to materials and devices, leading to on-orbit failures and even accidents of spacecraft. Developing lightweight and efficient radiation shielding materials is an effective approach to improve the inherent protection of spacecraft. The protective performance of different materials against proton and electron spectra in the Earth's radiation belts is evaluated by Geant4 simulation. Based on the simulation results, suitable hardening components are selected to design composite materials, and B_4C/PEEK composites with different B_4C content were successfully prepared. Experimental results demonstrate that the simulated and experimental results for the electron, proton and neutron shielding performance of B_4C/PEEK composites are consistent. These composites exhibit excellent radiation shielding capabilities against electrons, protons and neutrons, and the radiation protection performance improves with increasing B_4C content in the B_4C/PEEK composite materials.

Keywords: radiation shielding; simulation; hardening component; B_4C/PEEK; composite material

0. Introduction

In the space environment, there exist various types and energies of charged particles, mainly electrons and protons, which can cause radiation damage to spacecraft. As human space activities expand, spacecraft face increasingly stringent tests and challenges in terms of on-orbit service life and reliability [1]. Developing lightweight and efficient radiation shielding materials is an effective approach to provide intrinsic physical protection against radiation damage to spacecraft materials and components [2]. The radiation damage to spacecraft materials and components can be effectively reduced by directly blocking and absorbing the energy of external radiation particles by installing a certain thickness protective layer on the surface and around the spacecraft materials and components that are vulnerable to radiation damage [3,4].The development of lightweight and efficient radiation protection composite materials is one of the effective ways to reduce the radiation damage of airborne electronic components.

Among the top ten advances in the field of advanced materials in the foreign defense science and technology annual report for 2020, the research conducted at North Carolina State University in the United States reported on a polymer-based radiation protection composite material embedded with bismuth trioxide (Bi_2O_3) particles [5]. This radiation protection material is mainly based on ultraviolet irradiation curing method, composed of 44% bismuth trioxide added with polymethyl methacrylate (PMMA), which can effectively shield ionizing radiation such as gamma rays. It has the advantages of high strength, light weight, non-toxic and low cost, and is a potential substitute for traditional radiation protection materials such as lead and aluminum. It can be used in radiation protection for human space exploration, radiation therapy, medical imaging, and other applications [6,7]. This indicates that polymer-based radiation protection composite materials are receiving high attention from foreign researchers and are one of the current hotspots in radiation protection material research.

 doi:10.20944/preprints202409.1077.v1

Domestic researchers, such as Rui Erming et al., incorporated carbon nanotube reinforcement elements into Low-Density Polyethylene (LDPE) to produce radiation protection composite materials. Their study revealed that under the same mass thickness, MWCNTs/LDPE composite materials exhibited superior proton and electron radiation shielding capabilities compared to metallic aluminum. The high hydrogen content of LDPE polymers contributes to enhanced radiation protection performance. However, LDPE itself possesses weak radiation resistance, leading to susceptibility to damage in LDPE-based composite materials after radiation exposure.

In recent years, It has become a research hotspot in the field of aeronautics and astronautics to process new polymeric radiation shielding materials by adding nanoparticles with excellent radiation shielding properties into specific polymer substrates. Poly ether ether ketone (PEEK) boasts exceptional high-temperature resistance, aging resistance, mechanical properties, insulation stability, and radiation resistance, making it widely applicable in aerospace [8–11].

With the development of nanotechnology, micro-nano particle units and polymer matrix composites with good radiation resistance provide a new way to develop lightweight and efficient space radiation protection materials [12–15]. This includes incorporating high atomic number elements (excluding lead), metal oxides, and graphite nanofibers (or nanotubes) as secondary elements into polymer matrices [16]. Compared to metallic lead, polymer-based composite materials prepared with these elements demonstrate significant lightweight and efficient characteristics [17,18]. Additionally, exploratory work on adding other elements is underway, but it has yet to meet the application requirements for space radiation protection [19].

The key technological challenge in the development of polymer-based radiation protection materials lies in the uniformly incorporating micro-nano level particle materials into radiation-resistant polymer matrices and producing lightweight structures with specific forms [20].

Research on preparing radiation-resistant composite materials based on PEEK is still in its early stages. There is a lack of necessary design guidelines for radiation protection composite materials, and related manufacturing process technologies need to be explored from scratch [21]. In order to provide theoretical guidance and technical support for the development of new polymer radiation protection composites, the design concept, preparation and characterization of PEEK-based radiation protection composites reinforced by nanoparticles were deeply studied [22–24].

In essence, this means that basic principles and guidelines for the design of radiation-resistant composites based on PEEK need to be established. Researchers would need to explore various methods to incorporate nano-particles into PEEK matrices effectively. This involves investigating the properties and behavior of these materials under radiation exposure, as well as developing appropriate manufacturing processes to ensure the uniform distribution and effective reinforcement of nanoparticles within the polymer matrix. Additionally, comprehensive characterization techniques are necessary to evaluate the performance of these composites in terms of radiation shielding efficacy, mechanical properties, durability, and other relevant factors. Overall, this research direction aims to lay the groundwork for the development of advanced radiation protection materials using polymer composites based on PEEK.

1. Radiation Protection Composite Material Simulation, Calculation, and Design

1.1. Calculation of Shielding Effectiveness for Different Types of Materials and Selection of Matrices

Figure 1 illustrates the proton shielding effectiveness of different thicknesses of traditional space shielding material Aluminum (Al) and promising polymer materials Polyimide (PI), Poly ether ether ketone (PEEK), and Polyethylene (PE) for Low Earth Orbit (LEO) radiation belts (Orbit altitude 200-600 km, Inclination approximately 45°). Figure 1(b) represents the differential cumulative fluence for different materials at the same mass thickness. As observed from the graph, a significant reduction in the differential cumulative fluence compared to the LEO orbit spectrum, with better shielding effects achieved with thicker shielding layers. When comparing materials at the same thickness and proton energy, the proton differential cumulative fluence after polymer material shielding is slightly higher than that after Aluminum shielding, indicating that Aluminum provides better proton

 doi:10.20944/preprints202409.1077.v1

shielding effects compared to polymers such as PE, PEEK, and PI at the same thickness. However, Aluminum, being a metallic material, is heavier and less conducive to spacecraft weight reduction. As shown in Figure 1(b), calculations reveal that at the same mass thickness, the proton fluence after Aluminum shielding is higher than that after polymer material shielding, suggesting that polymer materials provide better proton shielding effects than Aluminum at the same mass thickness. Figure 1(a) indicates that PE exhibits slightly better shielding effectiveness than PI and PEEK, but aromatic PEEK and PI demonstrate significantly superior comprehensive properties in terms of mechanics, thermal, and electrical characteristics, particularly in their ability to withstand radiation damage, which surpasses that of PE. Moreover, at higher proton energies, the shielding effectiveness of Aluminum and various polymer materials is comparable.

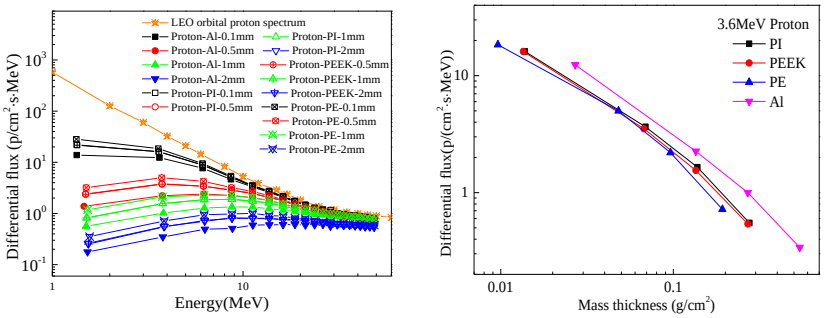

(**a**) (**b**)

Figure 1. Differential cumulative flux spectra of LEO orbital protons protected by different materials and the same mass thickness (a) Differential cumulative flux spectra after different material and thickness protection (b) Proton protection effect of different materials with the same mass thickness.

Figure 2 shows the differential cumulative fluence spectra of secondary neutrons and γ-rays after proton incidence through various thicknesses of shielding layers in the Low Earth Orbit (LEO). The depiction in the figure reveals that proton incidence on different shielding materials lead to the generation of secondary particles such as neutrons and γ-rays through nuclear spallation. The differential cumulative fluence of neutrons and secondary γ-rays produced by polymer materials is significantly lower compared to metallic Aluminum (Al), highlighting the effective reduction of secondary particle production by protons through the use of polymer materials. Research suggests that PEEK sheets exhibit strong resistance to radiation damage and show promise as a matrix material for polymer-based radiation protection. Considering these findings, PEEK is selected as the matrix for polymer-based radiation protection materials. However, it is acknowledged that a single material may not fully meet the varied spectrum of radiation protection requirements in space, underscoring the need for the development of lightweight and efficient radiation protection composite materials. Moreover, studies have indicated that composite materials created by integrating nano-particles into polymer matrices contain numerous interfaces that contribute to improving the radiation protection performance of the composites.

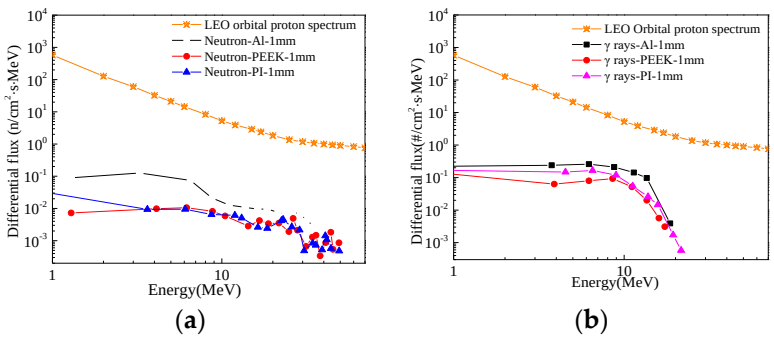

(**a**) (**b**)

 doi:10.20944/preprints202409.1077.v1

Figure 2. Differential cumulative flux spectra of secondary neutrons and gamma rays after LEO orbital protons pass through protective layers of different thicknesses (a) Secondary neutrons (b) γ rays.

1.2. Calculation of Protective Effect of Composite Materials and Selection of Reinforcement Components

As shown in Figure 3, the differential cumulative flux spectra of secondary gamma photons after 2mm different materials shielding layers in the GEO orbit is depicted. It can be observed from the graph that the secondary particles produced by 20wt% Ta/PI composite material are more than those produced by the metal Al. Therefore, metallic Ta is excluded as a filler. The B_4C/PEEK composite has a lower secondary photon differential cumulative flux. Based on the above factors, B_4C was selected as the strengthening component to prepare a new radiation shielding composite with different addition amounts of B_4C/PEEK.

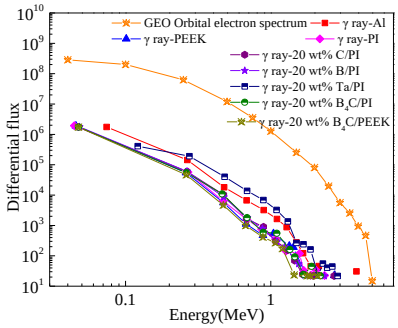

Figure 3. The differential cumulative flux spectra of the second gamma of GEO orbital electrons through 2 mm protective layer of different materials.

1.3. B_4C/PEEK Protection Effect Calculation

Figure 4 illustrates the simulated results of the protective effects against 1MeV electrons for different materials. In the graph, the thicknesses of PEEK, Al, and B_4C materials are 2mm, while PI material has a thickness of 25μm. Therefore, PI exhibits lower electron radiation protection compared to PEEK. It can be observed from the graph that B_4C offers the best electron protection, followed by metallic aluminum, then polymer PEEK and PI materials. However, both B_4C and metallic aluminum generate secondary particles after being irradiated by charged particles, and their high densities are unfavorable for spacecraft weight reduction.

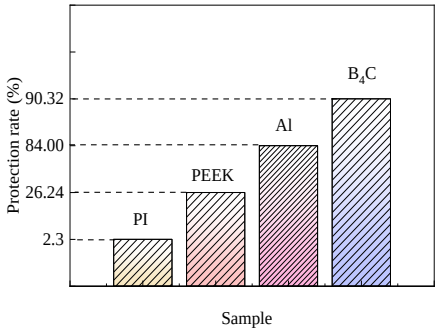

(**a**)

Preprints.org (www.preprints.org) | NOT PEER-REVIEWED | Posted: 13 September 2024 doi:10.20944/preprints202409.1077.v1

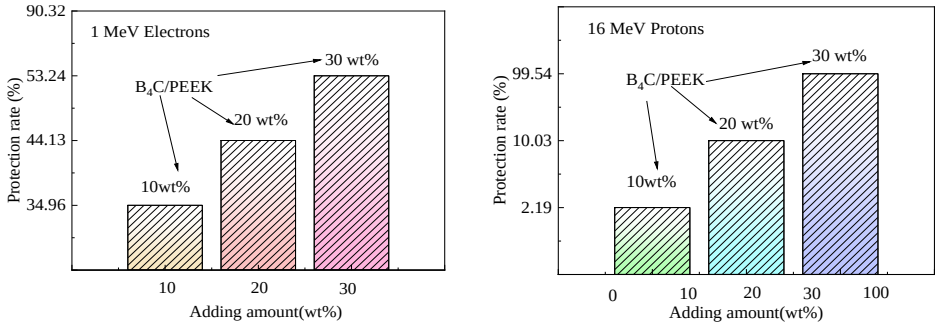

Figure 4. Simulation calculation results of 1 MeV electron and 16MeV proton protection rate of materials (a) Protective effect of different materials, (b) Electronic protective effect of B_4C/PEEK at different B_4C addition levels, and (c) 16MeV Proton protective effect of B_4C/PEEK at different B_4C addition levels.

By adding varying amounts of B_4C to the radiation-resistant PEEK matrix, lightweight and efficient radiation shielding B_4C/PEEK composite materials can be obtained. Adding too much B_4C adversely affects the mechanical properties of the composite material, while adding too little results in inadequate protection. Therefore, B_4C filler addition amounts of 10wt%, 20wt%, and 30wt% are designed for B_4C/PEEK composite materials.

Simulations of radiation protection rates against 1MeV electrons and 16MeV protons for different B_4C addition levels in B_4C/PEEK composite materials are shown in Figure 4 (b) and (c). The results showed that the protection rate of B_4C against 1MeV electron radiation was significantly improved after adding B_4C to B_4C/PEEK composites, and the greater the amount of B_4C added, the better the protection effect. This can be compared with experiments on electronic radiation protection. When the incident proton energy is high, such as 100MeV, B_4C/PEEK composite materials with different B_4C addition amounts cannot completely shield them. However, when the incident proton energy is lower, such as 3MeV and 10MeV, B_4C/PEEK composite materials can completely shield them. After adding B_4C, the proton radiation protection rate of B_4C/PEEK composite materials significantly increases with increasing B_4C addition after irradiation with 16MeV protons.

2. Preparation and Characterization of Experimental Materials

2.1. Test Materials and Equipment

The polyether ether ketone (PEEK) material used in the experiment, with a density of 1.35g/cm³ and a thickness of 50μm, is sourced from Victrex plc, United Kingdom. The boron carbide (B_4C) powder, comprising 95%, is sourced from the School of Chemical Engineering at Harbin Institute of Technology. The precision electronic balance, model number 124-1CN, is sourced from Suzhou SANS Instrument Co., Ltd. The electrically heated constant temperature drying oven, model number 500-02, is sourced from Hu Yue Instrument Equipment Factory in Shaoxing, Zhejiang Province, China. The planetary ball mill, model number YXQM, is sourced from Changsha Miqi Instrument Equipment Co., Ltd. The high-temperature press machine, model number HBSCR-100T, is sourced from Qingdao Bohua Technology Co., Ltd.

2.2. B_4C/PEEK Preparation Technology

Using compression molding, B_4C/PEEK composite materials with different B_4C addition levels were prepared. To achieve excellent radiation shielding performance, the key lies in enhancing the compatibility between the B_4C component and the PEEK matrix, as well as improving the dispersion of the added B_4C particles in the matrix. A certain amount of B_4C reinforcing component and a specific quantity of 200-mesh PEEK matrix particles were weighed using an electronic balance. After thorough mixing, the mixture was placed into a planetary ball mill for grinding. Following grinding, the B_4C and PEEK mixture exhibited exceptional homogeneity, with both the B_4C component and the

 doi:10.20944/preprints202409.1077.v1

PEEK matrix ground into nanoscale sizes. The preparation process for B_4C/PEEK using compression molding is illustrated in Figure 5. By separately weighing different amounts of B_4C reinforcing component and employing the aforementioned preparation technique, B_4C/PEEK composite materials with B_4C addition levels of 10 wt%, 20 wt%, and 30 wt% were successfully prepared.

Figure 5. Preparation flow diagram of B_4C/PEEK composite materials.

2.3. Characterization Method

The testing of electron radiation protection performance was conducted at the Institute of Technical Physics, Heilongjiang Academy of Sciences, using a high-frequency high-voltage electron accelerator. The energy of the electron beam was 1MeV. The proton radiation protection testing was carried out on the R20 branch of the HI-13 serial accelerator at Beijing, where the beam spot area was 50mm×50mm, and the non-uniformity of the beam spot distribution was better than 10. Various energy single-energy proton beams (energy resolution less than 10^{-3}) were used to irradiate B_4C/PEEK test specimens, with energy ranging from 12MeV to 20MeV. During irradiation, the proton beam intensity was controlled to be around 2.0×10^4 p/s, and the irradiation time for each individual specimen exceeded 100s. The neutron radiation protection testing was conducted at the Small Angle Spectrometer of the Dongguan Chinese Spallation Neutron Source, using B_4C/PEEK composite material samples.

3. Radiation Protection Result

3.1. Electronic Radiation Protection Effect

The electronic radiation protection properties of B_4C/PEEK composites were tested at a 1MeV electron irradiation dose of 2×10^{14}e/cm². According to the absorbance data obtained by the thin film dosimeter and compared with the standard provided by the measuring institution, the absorbed dose of irradiation is calculated using equation (1).

$$D = 5.45023X^{1.15071}$$
$$\mathrm{X} = \frac{A - A_0}{42.5} * 1000 \quad (1)$$

D——Radiation absorbed dose；

X——Absorbance per unit thickness；

A——The absorbance value of a radiation-changing film dose-piece after irradiation；

A_0——The background absorbance value of the radiation-changing film dose tablet before irradiation。

The smaller the absorbed dose measured in the experiment, the better the electron radiation protection effect of the composite material being tested. Figure 6 shows the absorbed dose distribution curves of B_4C/PEEK composites with different B_4C addition amounts along the depth of the film dosimeter under electron irradiation. It can be observed that the absorbed dose of the PEEK material's thin film dosimeter is higher than that of the surface dosimeter at a depth of 2mm. This difference occurs because 1MeV electrons penetrate the dosimeter and the material at a depth of 0mm, while the electrons in PEEK materials have a range of about 2mm, allowing the deposited

 doi:10.20944/preprints202409.1077.v1

energy to accumulate in the PEEK material. Therefore, with changes in electron energy upon entering the material and the generation of secondary particles, an increase in dose occurs at the depth of 2mm.

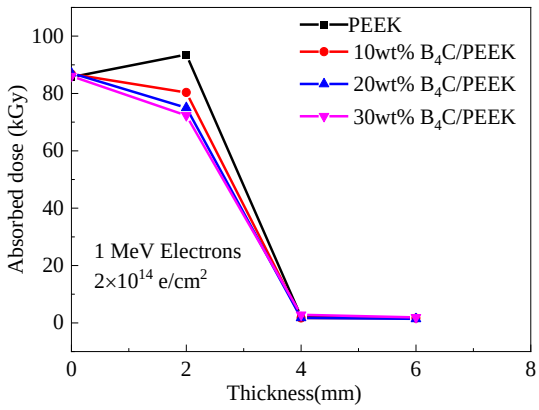

Figure 6. Distribution curves of film dose tablets along the thickness of B_4C/PEEK under electron irradiation.

The absorbed doses of B_4C/PEEK composite materials with different B_4C addition levels are lower than those of surface dosimeters and significantly lower than the doses absorbed by dosimeters at 2mm depth in PEEK. Additionally, they are lower than the absorbed doses of B_4C/PEEK surface dosimeters, indicating the protective effect of B_4C/PEEK composite materials. This suggests that with an increase in the B_4C addition level, the electron radiation protection effect strengthens.

When the total shielding layer thickness is 4mm, the dosimeter test results indicate an absorbed dose of approximately 1.5kGy for electron irradiation. This is the background absorbed dose for the dosimeter before irradiation, indicating that the electrons are completely shielded and the transmittance is 0. Therefore, the thickness of the material significantly affects the electron radiation protection effect.

3.2. Proton Radiation Protection Effect

The proton transmission rate curves with energy variation for composite materials with different B_4C addition levels show In Figure 7. In Figure 7(a), the sample corresponds to 10wt% B_4C/PEEK. It can be observed from the graph that when the energy exceeds 14 MeV, the incoming protons mostly penetrate through, and the proton transmission rate significantly decreases as the energy decreases, indicating a noticeable increase in protection. At 12MeV, the proton transmission rate decreases to 52%. Based on this trend, it is inferred that for complete shielding of incoming protons, their energy should be below 10MeV. The curve obtained by fitting the data points follows the trend of decreasing protection with increasing energy, indicating the correctness of the experimental results. The red dashed line in the graph represents the differential curve of the fitted curve, indicating the cutoff energy range of the material. Figure 7 (b) illustrates the proton transmission rate curve with energy variation for 20wt% B_4C/PEEK composite material. It shows a significant decrease in proton transmission rate with decreasing energy, with protons below 16MeV being essentially shielded and those above 18MeV being mostly penetrable. This indicates an average cutoff energy of 17MeV for this composite material. Comparing the results of proton radiation protection for composite materials with 10wt% and 20wt% B_4C additions reveals a significant increase in the energy of shielded protons, from 10MeV to 16MeV. Therefore, B_4C/PEEK composite materials with added B_4C components exhibit significantly enhanced proton shielding effectiveness.

 doi:10.20944/preprints202409.1077.v1

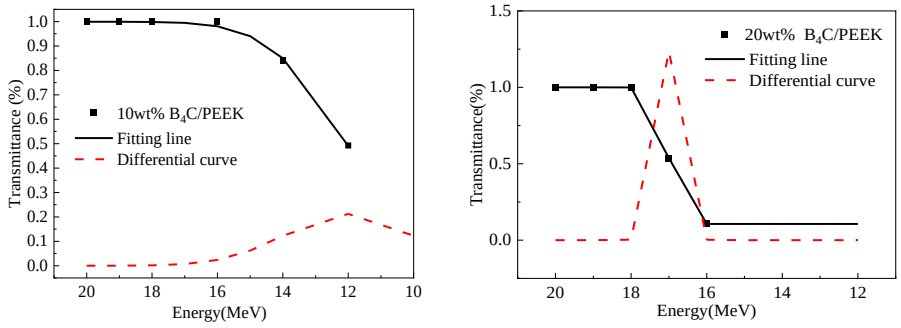

Figure 7. Protons transmittance of B_4C/PEEK composites change with energy (a) 10 wt% B_4C/PEEK, (b) 20 wt% B_4C/PEEK.

3.3. Neutron Radiation Protection Effect

The neutron radiation protection testing curves for PEEK and B_4C/PEEK composite materials with different B_4C addition levels show in Figure 8. In Figure 8(a), the relationship between neutron counts and wavelength is shown, while Figure 8(b) illustrates the relationship between protection effectiveness and wavelength. The formula (2) calculates the relationship between neutron flight time and neutron wavelength:

$$\tau=\frac{m_n\lambda L}{h} \tag{2}$$

h——Planck's constant;
m_n——Mass of neutron;
τ——Flight time;
L——The distance the neutron travels from the chopper to the GEM detector。

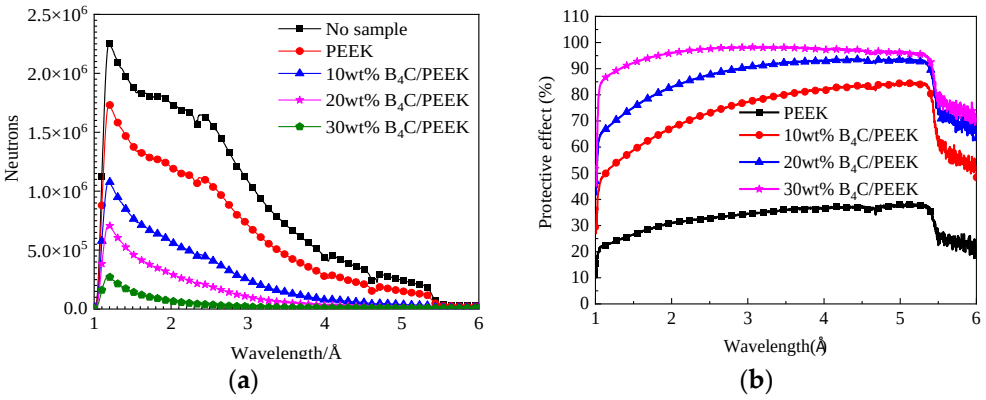

Figure 8. Neutron protection curves of B_4C/PEEK composite materials with different B_4C addition amount (a) Variation curve of neutron count and wavelength (b) Change curve of wavelength and protection effect.

According to Equation (2), the relationship between flight time and neutron counts can be transformed into the relationship between neutron wavelength and neutron counts, as shown in Figure 8. In Figure 8(a), the neutron counts versus wavelength relationship for B_4C/PEEK composite materials with different B_4C addition levels is illustrated, while Figure 8(b) displays the relationship between protection effectiveness and wavelength. From the graphs, it can be observed that PEEK material exhibits some level of neutron protection effectiveness. After incorporating B_4C reinforcing components, the neutron protection effectiveness of the composite material significantly increases, with greater addition amounts resulting in better neutron shielding. When the B_4C addition level reaches 30wt%, the neutron counts of the sample approach zero for neutron wavelengths greater than 3.1Å.

 doi:10.20944/preprints202409.1077.v1

Comparing the neutron counts of composite materials with different B_4C contents reveals that the critical wavelength at which neutrons are completely shielded decreases with the B_4C addition level increase. Additionally, it can be observed that the neutron count peaks around 1 Å wavelength and around 2.5Å wavelength decrease with increasing B_4C content in the sample, and the critical value at which neutrons are completely shielded shifts towards smaller angles with increasing B_4C addition, indicating a significant enhancement in neutron protection effectiveness after adding B_4C components. This is mainly attributed to the high slow neutron absorption cross-section of the ^{10}B element in B_4C, making it easier for larger-wavelength neutrons to be absorbed by the B_4C/PEEK composite material. For B_4C/PEEK composite materials, when the B_4C addition level increases from 10wt% to 30wt%, a significant amount of neutrons with wavelengths of 2.5Å and longer are absorbed. This results in a relatively lower count rate of the GEM detector per unit time, leading to a decrease in count peaks.

4. Conclusion

The Geant4 program simulation results indicate that PEEK has better radiation protection performance against charged particles than aluminum at the same mass thickness. The addition of B_4C components effectively enhances the radiation protection performance of polymer-based composite materials. By adjusting the process parameters, B_4C/PEEK radiation protection composite materials with different B_4C addition levels were successfully prepared.

The simulation results of electron and proton radiation protection of B_4C/PEEK composites are consistent with the experimental results, showing excellent proton radiation protection ability. In addition, with the increase of B_4C addition, the radiation protection performance improved. The electron, proton and neutron radiation protection properties of B_4C/PEEK composites were enhanced with the increase of B_4C content.

Funding: ational Natural Science Foundation of China Youth Project "Study on the Generation and Evolutionary Behavior of Proton Irradiation Defects in Temperature-dependent $CsPbBr_3$ Quantum Dots" (Project No. 12305310).

References

1. CAO Lei, Ke Yubin, Tao Juzhou et al. Preparation and Properties of Boron carbide/Polytetrafluoroethylene neutron absorption composites [J]. Materials Science, 2018, 8(6).
2. herkashina N I, Pavlenko V I, Noskov A V. Radiation Shielding Properties of Polyimide Composite Materials[J]. Radiation Physics and Chemistry, 2019, 159: 111-117.
3. Mcmillan J. Radiation Shielding Composites using Thermoplastic Polymers Mouldable at Low Temperature. 2019, 8(15), 05197.
4. Wang H, Hang Z, Yu S, et al. Preparation and Radiation Shielding Properties of Gd_2O_3/PEEK Composites[J]. Polymer Composites, 2014, 36(4).
5. Rui Erming. Effects and mechanism of low-energy proton and electron irradiation of LDPE/MWCNTs composites [D]. Harbin: Harbin Institute of Technology, 2013, 178-183.
6. Li R, Gu Y, Zhang G, et al. Radiation Shielding Property of Structural Polymer Composite: Continuous Basalt Fiber Reinforced Epoxy Matrix Composite Containing Erbium Oxide[J]. Composites Science and Technology, 2017, 143(MAY3): 67-74.
7. Srinivasan K, Samuel E J. Evaluation of Radiation Shielding Properties of the Polyvinyl Alcohol/Iron Oxide Polymer Composite[J]. Journal of Medical Physics, 2017, 42(4): 273-278.
8. Wu Enthan. Preparation and electromagnetic shielding properties of lightweight polyether ether ketone composites [D]. Jilin: Jilin University, 2020, 12-13.
9. Rival G, Paulmier T, Dantras E. Influence of Electronic Irradiations on the Chemical and Structural Properties of PEEK for Space Applications[J]. Polymer Degradation and Stability, 2019, 168: 108943.
10. Lu C R, Wang J, Lu X. PAI/MXene Sizing-based Dual Functional Coating for Carbon fiber/PEEK Composite[J]. Composites Science and Technology, 2020, 201.

 doi:10.20944/preprints202409.1077.v1

11. Kadiyala A K, Bijwe J. Poly (ether ether ketone) - Silicon Carbide Composite Adhesives for Elevated Temperature Applications of Stainless Steel Joints[J]. Composites Science and Technology, 2017, 155(8): 177-188.
12. Yan S, Wang A, Fei J, et al. Hydrogen Ion Induced Ultralow Wear of PEEK under Extreme Load[J]. Applied Physics Letters, 2018, 112(10): 101601.
13. Jap A, Mc B, Jam A, et al. Tribological and Mechanical Properties of Graphene Nanoplatelet/PEEK Composites - ScienceDirect[J]. Carbon, 2019, 141: 107-122.
14. Jwt A, Cyl A, Yky A, et al. Screw Extrusion-based Additive Manufacturing of PEEK[J]. Materials & Design, 2018, 140: 209-221.
15. Awaja F, Zhang S, James N, et al. Enhanced Autohesive Bonding of Polyetheretherketone (PEEK) for Biomedical Applications Using a Methane/Oxygen Plasma Treatment[J]. Plasma Processes & Polymers, 2015, 7(12).
16. Jahan M S, Walters B M, Riahinasab T, et al. A Comparative Study of Radiation Effects in Medical-grade Polymers: UHMWPE, PCU and PEEK[J]. Radiation Physics and Chemistry, 2015:456(2): 74.
17. Reitman M, Jaekel D, Siskey R, et al. Chapter 4–Morphology and Crystalline Architecture of Polyaryletherketones[J]. PEEK Biomaterials Handbook (Second Edition), 2019: 53-66.
18. Pu L, Huang X, Wang W, et al. Strategy to Achieve Ultralow Dielectric Constant for Polyimide: Introduction of Fluorinated Blocks and Fluorographene Nanosheets by in Situ Polymerization[J]. Journal of Materials Science: Materials in Electronics, 2019, 30(15): 14679-14686.
19. Song N, Yao H, Ma T, et al. Decreasing the Dielectric Constant and Water Uptake by Introducing Hydrophobic Cross-linked Networks into Co-polyimide Films[J]. Applied Surface Science, 2019, 480(6): 990-997.
20. Pantoja M, Boynton N, Cavicchi K A, et al. Increased Flexibility in Polyimide Aerogels Using Aliphatic Spacers in the Polymer Backbone[J]. Acs Applied Materials & Interfaces, 2019, 45(3): 23-29.
21. Tkachenkoa I, Kononevichb Y, Kobzara Y, et al. Low Dielectric Constant Silica-Containing Cross-linked Organic-inorganic Materials Based on Fluorinated Poly(arylene ether)s[J]. Polymer, 2018, 157(4):131–138.
22. Dutta N J, Mohanty S R, et al. Self-organized Nanostructure Formation on the Graphite Surface Induced by Helium Ion Irradiation[J]. Physics Letters A, 2018, 382(24): 1601-1608.
23. Chand S. Influence of B_4C/BN on Solid Particle Erosion of Al6061 Metal Matrix Hybrid Composites Fabricated Through Powder Metallurgy Technique[J]. Ceramics International, 2020, 46(11).
24. Lu Y, Zhang Q, Xue Y, et al. High-Velocity Impact Performance of Aluminum and B_4C/UHMW-PE Composite Plate for Multi-Wall Shielding[J]. Applied Sciences, 2020, 10(2): 721.